# Fresh-Water/Sea-Water Relationship Within a Ground-Water Flow System, Northeastern Coast of the Yucatan Peninsula

by Yolanda H. Moore, Ronald K. Stoessell, and Dale H. Easley[a]

## Abstract

**Ground-water velocities within fractures and boreholes, hydraulic heads, and depth profiles of conductivity were measured along a 70 km section of the northeastern coast of the Yucatan Peninsula, Mexico. Hydraulic heads ranged from 40 to 60 cm above mean sea level between 2 and 4 km from the coast. Fluid velocities estimated from point-dilution tests, in the dual-porosity rock in a borehole several kilometers from the coast, were 0.021 cm/sec in the fresh-water lens and 0.082 cm/sec near a fracture in the underlying sea-water zone. Velocities in large fractures increased from 1 cm/sec 10 kilometers inland to 12 cm/sec near discharge points along the coast. This increase is attributed to the decrease in thickness of the fresh-water lens.**

**The thickness of the fresh-water lens is approximately 40% less than the Ghyben-Herzberg relation predicts for a static system, providing the potential to drive fresh water through fractures into the sea-water zone below the halocline. Overall, the halocline appears to be in a steady-state position due to the rapid flow of fresh water and brackish water towards the coast combined with rising sea water in convectional flow.**

## Introduction

Ground-water mixing-zone data in coastal carbonate rocks are needed to model carbonate dissolution as a function of time and fluid flow (Sanford and Konikow, 1989a; 1989b; 1989c). The 70 km coastal region between Playa del Carmen and Tulum on the northeastern coast of the Yucatan Peninsula of Mexico (Figure 1), has been extensively studied by petrologists and geochemists and therefore is ideal for collecting the needed data on water-rock interaction. Aragonite dissolution probably occurred in this region in Pleistocene mixing zones (Ward and Halley, 1985) and occurs today (Back et al., 1986; Stoessell et al., 1989). Dolomite formed in the saline portion of the Pleistocene mixing zone but has not been found forming in the modern mixing zone (Ward and Halley, 1985; Stoessell et al., 1989).

Modeling carbonate rock dissolution in the mixing zone requires linking ground-water flow with geochemical interactions. Sanford and Konikow (1989a) applied their coupled hydrology-geochemical model to the Yucatan coast using the geochemical data taken from Back et al. (1979) at Caleta Xel-Ha north of Tulum (Figure 1). Sanford and Konikow noted that "no field areas are known that have the requisite data describing porosity and permeability distributions in sufficient detail to provide an unequivocal calibration" for their numerical model. Wilson (1989) pointed out that their model did not reproduce observed salinity-depth distributions nor take into account fracture flow velocities. Wilson's points are valid; however, Sanford and Konikow could not calibrate their model in the absence of published data on ground-water flow for this section of the Yucatan coast.

The objectives of this paper are to describe the ground-water flow system along the northeastern Yucatan coast and provide ground-water flow data that could be used to calibrate coupled ground-water flow/dissolution models such as that proposed by Sanford and Konikow (1989b). We report measured hydraulic heads, depth profiles of sea-water percent, and ground-water flow velocities from boreholes and fractures.

## Hydrogeology

This study covers the 70 km distance between Playa del Carmen and Tulum along the northeastern coast of the Yucatan Peninsula (Figure 1). The area is part of a flat, low-relief limestone platform characterized by minimal soil cover and rapid infiltration of rain water. The rainy season occurs from June through December with minimal rainfall occurring during the rest of the year. The average annual rainfall is 105 cm/yr of which 85% returns by evapotranspiration and the remainder becomes ground water (Back, 1985). Dissolution of carbonate rock has created a karst topography with sinkholes (cenotes) that are generally

[a]Department of Geology and Geophysics, University of New Orleans, New Orleans, Louisiana 70148.

Received March 1991, revised June 1991, accepted July 1991.
Discussion open until November 1, 1992.

found along fractures reflecting regional north-northeast-trending normal faults (Weidie, 1985). The coast contains crescent-shaped inlets (caletas) and beaches created by dissolution of carbonate rock where brackish water discharges into the Caribbean Sea (Back et al., 1979).

Carbonate rock within this karst terrain consists of Pleistocene limestones composed of low-Mg calcite, aragonite, and minor amounts of dolomite (Ward and Halley, 1985). Aragonite is undergoing active dissolution in the brackish water of the mixing zone (Back et al., 1986). This dissolution is not limited to the fresher, brackish water but extends throughout the saline portion of the mixing zone (Stoessell et al., 1989). Megaporosity in thin sections varies from 20 to 60% (Stoessell et al., 1989). The bulk-rock porosity of these limestones consist of both pores and open fractures (here referred to as "dual porosity").

There are two types of flow systems in the unconfined aquifer, with gradations in between, operating in this coastal area: a porous-medium system and a fracture system. The phreatic water column is divided into three regimes, as represented in Figure 2. A fresh-water lens, resulting from the infiltration of rain water, lies above a brackish-water zone, which overlies sea water. The fresh water typically has less than 5% of the salinity of sea water. The halocline is the region of most rapid change in salinity with depth, generally from 5 to 95% sea-water salinity, and defines the brackish-water zone (Figure 2). The ground water underlying the brackish water is referred to as sea water because its origin is the Caribbean Sea and it has the general composition and salinity of sea water.

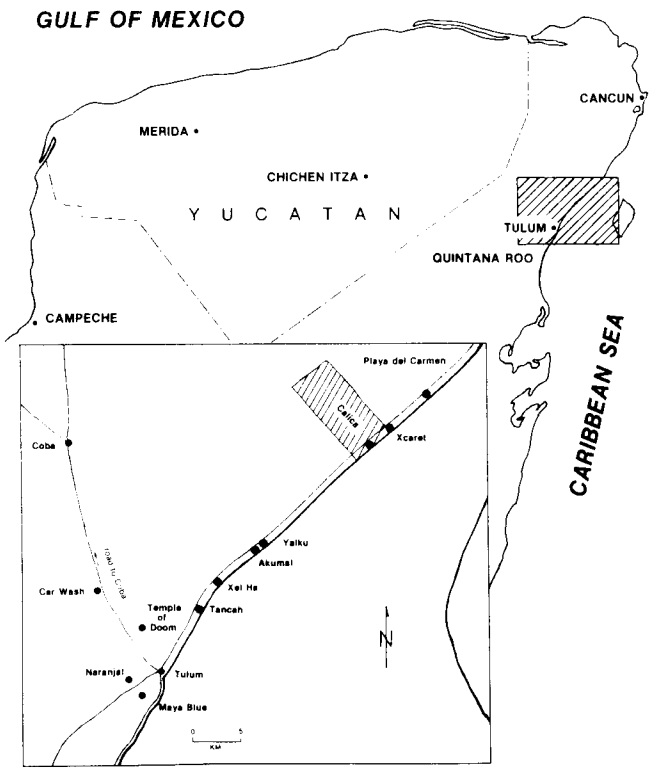


**Fig. 1. Locations of study sites along a 70 km section of the Yucatan coast between Playa del Carmen and 2 km south of Tulum.**

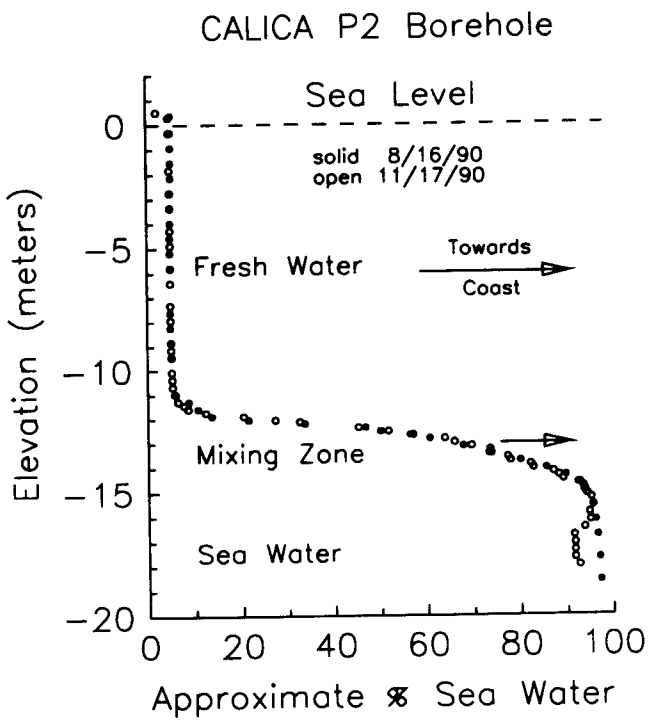


**Fig. 2. Depth profiles of sea-water percent for P2 borehole in August and November 1990.**

The brackish-water zone forms from mixing of fresh water and sea water and increases in vertical thickness approaching the coast. Waters in the fresh-water lens, brackish-water zone, and in the upper portion of the underlying sea water beneath the brackish-water zone flow towards the coast; whereas, with depth there is a net movement of sea water inland to account for the brackish water formed in the mixing zone (Cooper, 1959). The sea water rises because of the decrease in density due to mixing with fresh water. Whitaker and Smart (1990) have proposed this "buoyant circulation" process as possibly occurring under the Great Bahama Bank.

## Site Locations and Methods

The study utilized boreholes and cenotes in the coastal region extending from Xcaret to 2 km south of Tulum (Figure 1). Nine boreholes and one cenote (sinkhole) are on CALICA property, an industrial site extending from the coast to about 10 km inland and located 8 km south of Playa del Carmen. The inland cenotes are Car Wash, Temple of Doom, Maya Blue, and Naranjal. Those adjacent to the coast are at Xcaret, Yalku, and Tancah, used by Stoessell et al. (1989). The Yalku site is an open-surface fracture located 100 meters from the northeast side of the caleta. The discharge point of this fracture into the caleta is the Yalku study site of Stoessell et al. (1989).

### *CALICA Boreholes and Cenote*

Measurements taken within the CALICA boreholes and cenote in August and November 1990 included the hydraulic heads (relative to mean sea level) and depth profiles of conductivity and temperature. Grid locations for the

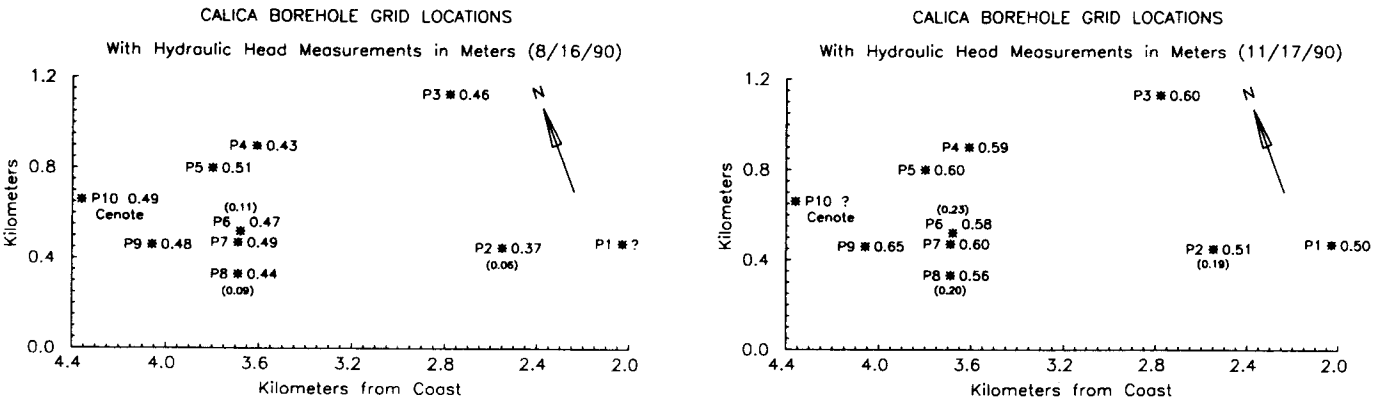


**Fig. 3. Grid locations and fresh-water hydraulic head measurements of CALICA boreholes and cenote: (3a) in August 1990; and (3b) in November 1990. Several computed sea-water hydraulic heads are listed in parentheses.**

nine boreholes are shown on Figure 3, together with the location of the CALICA cenote. The boreholes were uncased in August and, with the exception of the P2 and P1 boreholes, subsequently screened in November with perforated casing. Because of collapsing wellbores, complete depth profiles of conductivity and temperature were made in only half the boreholes.

A modified YSI model 3000 TLC temperature-conductivity meter with 50 meters of cable was used in measuring the depth profiles at the CALICA sites and elsewhere. The temperature profiles at the CALICA sites ranged between 24 and 26°C. The meter was modified to cover the salinity range of fresh water to sea water, resulting in measured laboratory errors of up to 4% in conductivity at 25°C without significant loss in linearity. Because the conductivity was used to estimate the sea-water percentage in mixtures of fresh water and sea water, the error was compensated for by setting the measured (maximum) conductivity in the sea-water zone to pure sea water and assuming a linear relation in mixtures of sea water and fresh water. Borehole water samples taken from P2, analyzed in the laboratory, indicated insignificant error in this assumption. In practice, field conductivity values less than 2.5 mmho/cm characterized the fresh-water compositions. The field sea-water conductivity was dependent on temperature and was approximately 51 mmho/cm.

In the uncased P2 borehole, a point-dilution method (Drost et al., 1968) was used in November to measure ground-water velocities in the fresh-water and sea-water zones (Figure 2). Two liters of sea water were introduced at 6.1 m below mean sea level (within the fresh-water lens). The subsequent decline in conductivity to the baseline fresh-water conductivity prior to injection was monitored with time. In the sea-water zone, four liters of fresh water were injected at a point 16.5 m below mean sea level, and the subsequent rise in conductivity to the baseline ground-water conductivity was monitored with time. In both cases the fluids were introduced from the surface through tubing attached to the conductivity probe cable and extending 0.6 m below the probe. Subsequently, the probe was lowered to the point of release and the test begun after the conductivity readings had stabilized. The conductivity value at the beginning of each test was within 2 mmho/cm of the baseline conductivity of the ground water before injection, producing a negligible difference in density of 0.001 g/cm$^3$. The velocity "v" is computed from

$$v = -(\pi r f/2t)\ \ln[(c - c^*)/(c^\circ - c^*)] \qquad (1)$$

where r is the radius of the borehole (9.1 cm); f is an empirical correction for the influence of the well on ground-water flow; c is the conductivity at time "t;" c° is the conductivity at t equals zero after injection; and c* is the baseline conductivity before injection. The original equation was presented by Drost et al. (1968) for the injection of a tracer which had zero concentration in the ground water. To account for the baseline conductivity of the ground water not being zero, $\ln[(c - c^*)/(c^\circ - c^*)]$ has replaced $\ln(c/c^\circ)$ in the original equation. The factor "f" was set to one because the well was not cased, screened, or packed and there were no data on "f" for uncompleted wells. A future study of the accuracy of this assumption is planned. The predicted linear relationship between time and $\ln[(c - c^*)/(c^\circ - c^*)]$ was observed in the field data until c approached the limiting value c*.

### *Cenotes in the Coastal Region*

Conductivities, temperatures, and ground-water velocities were measured as a function of water depth in the cenotes. With the exception of the open fracture utilized at Yalku, the measurements were taken at the openings of submarine caves leading into the cenotes. A Marsh-McBirney Model 201 velocity flow meter was used with a sensor on a 6 m cable attached to survey rods. The rods acted to stabilize the sensor during rotation to determine the direction of maximum velocity. The flow meter's sensitivity was 0.3 cm/sec, and its accuracy was within 1 cm/sec. The calibration of the flow meter was checked visually using a stop watch during several rhodamine B dye-tracer tests of horizontal flow at Yalku.

## Results and Discussion

All field data presented here in condensed form can be obtained upon request from the senior author. The complete data set is included in her thesis (Moore, 1991).

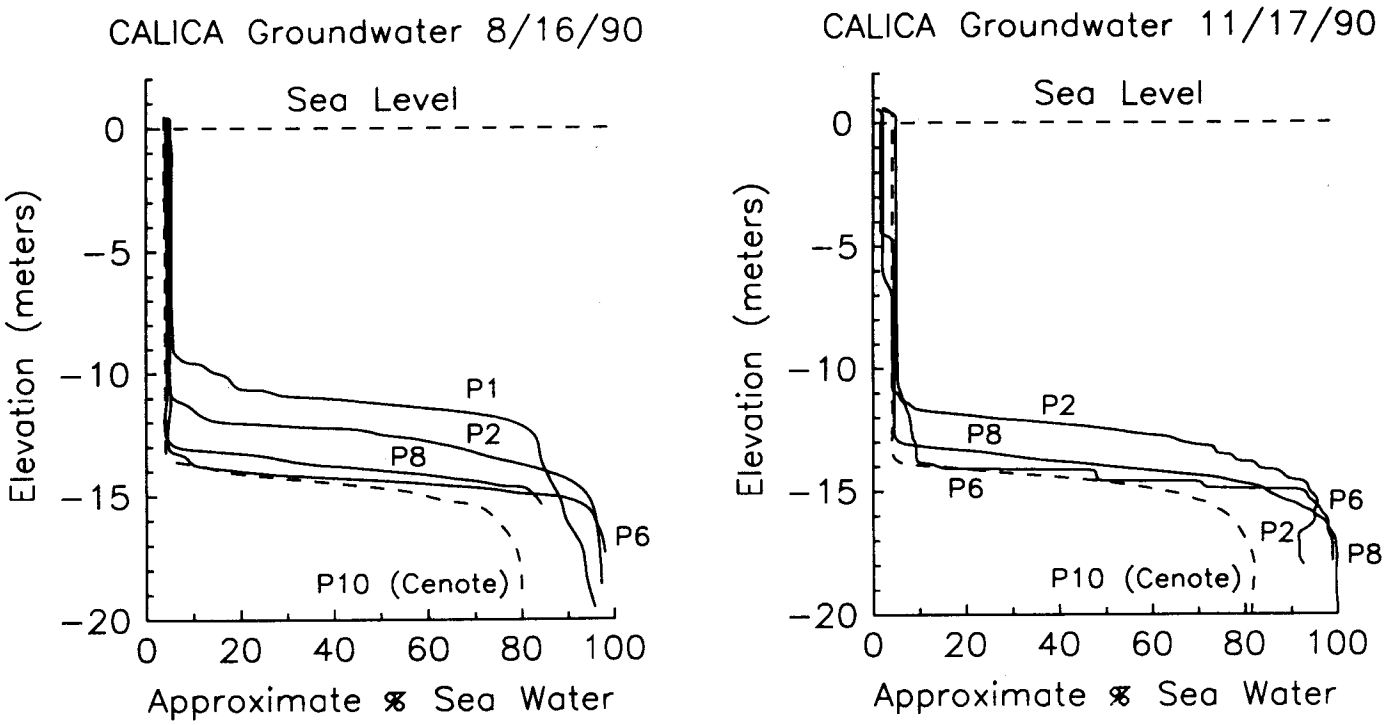


**Fig. 4. Depth profiles of sea-water percent for CALICA boreholes: (4a) in August 1990; and (4b) in November 1990.**

### *Hydraulic Heads*

Fresh-water hydraulic heads in meters above mean sea level for August and November are plotted on Figures 3a and 3b, respectively, for the CALICA boreholes. The benchmark elevations at the surface of each borehole were surveyed in by CALICA engineers and were measured from Mexican government established benchmarks for mean sea level. The accuracy of the conclusions from the hydraulic head data collected in this study area is dependent upon the accuracy of the established surveyed benchmarks. The hydraulic heads ranged from 37 to 51 cm in August and from 50 to 65 cm in November over approximately 2 km. The gradients indicate flow in a southerly direction towards the coast which lies due east-southeast of the borehole sites. The irregular head pattern and the oblique coastal flow direction are due to the influence of the regional north-northeast-trending fractures.

### *Depth Profiles of Sea-Water Percent*

Depth profiles of sea-water percent for the CALICA boreholes and cenote are shown in Figures 2 and 4 and are correlated on Figure 5. The profiles for the CALICA cenote reflect fracture flow in which increased dispersion has enlarged the brackish-water zone. The fresh-water hydraulic heads increased from August to November (see Figure 3), due to higher rainfall in the fall. These increases did not result in significant changes in the positions of the fresh-water, brackish-water, and sea-water zones, as shown in the P2 borehole in Figure 2. As discussed below, the thickness of the fresh-water lens is much thinner than expected for the measured fresh-water hydraulic heads.

Dispersion along the flow path in the porous medium increases the thickness of the brackish-water zone approaching the coast. This increase is shown on Figure 4 by comparing the thickness of the halocline from P6 (furthest from the

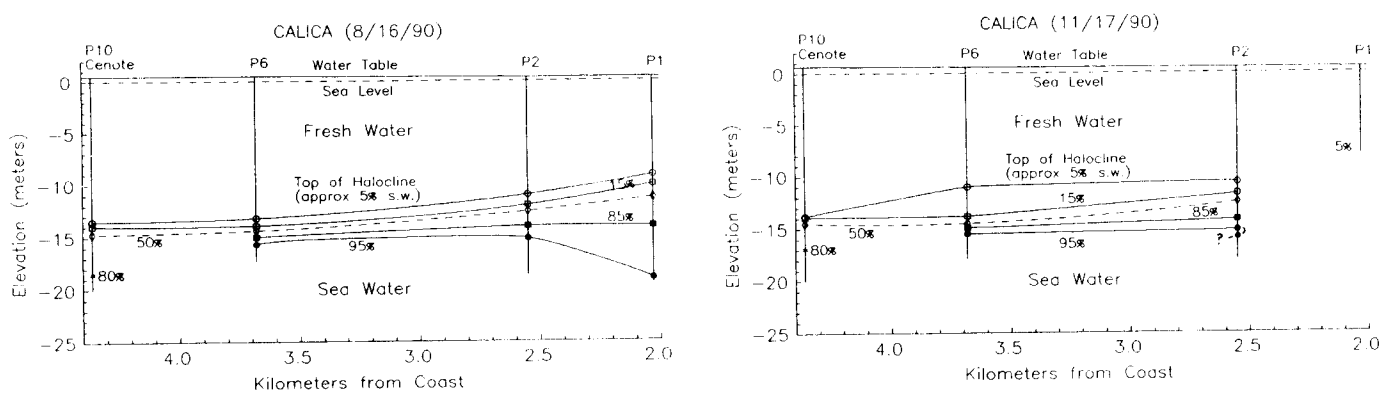


**Fig. 5. West-northwest to east-southeast cross section of phreatic zone at CALICA: (5a) in August 1990; and (5b) in November 1990.**

coast) to P8 to P2 to P1 (closest to the coast). The enlargement is shown more clearly in Figure 5 by the salinity isoclines approaching the coast. The increased width of the 5 to 15% sea-water zone in P6 during November may be due to increased turbulence in fracture flow resulting from increased rainfall.

In general, the depth profiles of sea-water percent imply water from the fresh-water lens simply mixes with water from the underlying sea-water zone to form brackish water in the halocline. However, as mentioned above, the thickness of the fresh-water lens did not significantly increase from August to November, even though there were increases in fresh-water hydraulic head. The thickness of the fresh-water lens at a borehole is much less than that predicted by the Ghyben-Herzberg relation for a static system with a sharp interface between the fresh-water and sea-water zones:

$$p_s z = p_f(z + h_f) \qquad (2)$$

where $p_s$ and $p_f$ are the densities of sea water and fresh water, respectively; $h_f$ is the fresh-water hydraulic head relative to mean sea level; and z is the vertical thickness of the fresh-water lens below mean sea level at the borehole site. Overestimation of the thickness of the fresh-water lens by the Ghyben-Herzberg relation is opposite to the underestimation usually produced by applying the relation to a real system having fluid flow (Freeze and Cherry, 1979, p. 376). Adding the total thickness of the brackish-water zone (1 to 2 m) to the thickness of the fresh-water zone does not substantially improve agreement with that predicted by the Ghyben-Herzberg relation.

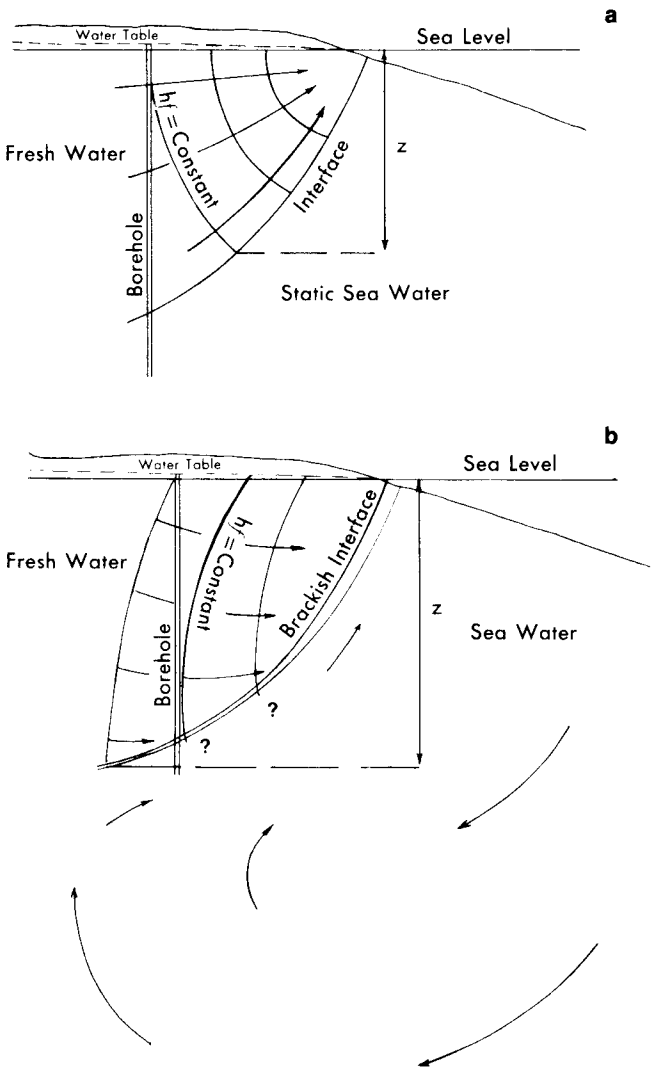


**Fig. 6. Schematic drawing showing changes in the phreatic zone approaching the coast: (6a) for dynamic equilibrium with moving fresh water overlying static sea water; and (6b) a hypothetical dynamic steady state with moving fresh water overlying moving sea water in which the fresh water is crossing the interface to create a brackish-water zone. Figure 6a and the sea-water convection cell in Figure 6b are modified from Cooper (1959).**

The assumption of static fresh water in the Ghyben-Herzberg model is removed in the Hubbert model (Hubbert, 1940) while retaining the assumptions of static sea water, a sharp interface, and no flow across the interface. The predicted vertical thickness of the fresh-water zone becomes dependent upon the curvature of the equipotential lines (Figure 6a) in Hubbert's model. The equipotential lines are no longer vertical and are concave upward towards the coast with increasing depth (Figure 6a). The vertical thickness z in equation (2) is now measured above the interface where the equipotential line from the water table in the borehole intersects with the interface (Hubbert, 1940). We did not have cased boreholes to define this point. However, because $h_f$ is too large for the measured thickness of the fresh-water lens, the equipotential lines must be concave downward to the interface to provide the hydraulic potential for fresh water to cross the interface. This is shown schematically in Figure 6b, indicating the thickness z to be greater than the vertical thickness of the fresh-water lens measured at the borehole. Therefore, the discrepancy between the measured thickness of the fresh-water lens and the thickness predicted by Hubbert's model has increased when compared to the Ghyben-Herzberg model. The ground-water system in the study area does not fit the assumptions of either model; however, by comparing our results with their predictions, we can see the effects of moving sea water, the development of a brackish-water zone, and flow across the interface.

The measured thickness of the fresh-water lens (including half of the brackish-water zone) in Figures 2 and 4 is approximately 40% less than predicted from equation (2) for the static system, using the hydraulic heads on Figure 3. These calculations assume densities of 1.025 g/cm$^3$ and 1 g/cm$^3$ for sea water and fresh water, respectively. This discrepancy is maintained by a dynamic balance between rapid flow of fresh water towards the coast and vertical upward movement in the sea-water zone (discussed below).

Injection of fresh water below the brackish-water zone will lower the fresh-water hydraulic head, moving the thickness of the fresh-water lens in the direction predicted for the static system. Evidence for this process occurring is shown in the November data on Figure 4b by the abrupt changes in salinity with depth in the brackish-water zone of P6 and the decrease in salinity within the sea-water zone in P2 (the

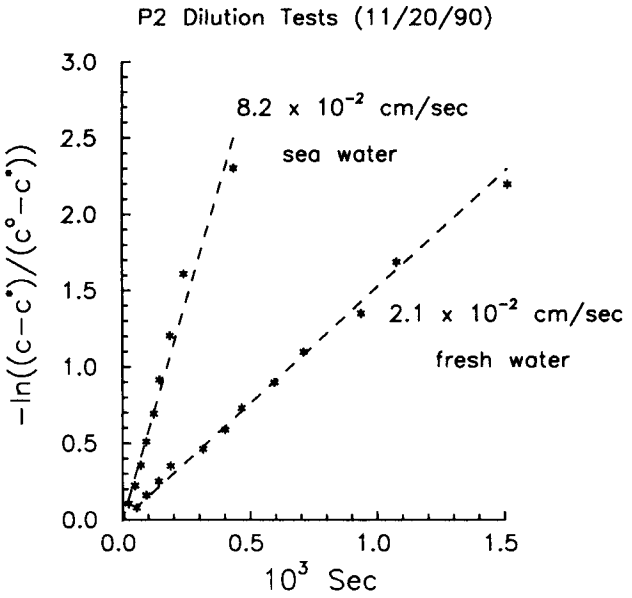


**Fig. 7. Point-dilution velocity tests taken in P2 borehole November 1990.**

notch on the diagram in Figure 2). Presumably, the notch reflects the downward flow of fresh water through fractures penetrated by the P2 borehole and explains the high velocity measured at this point in P2. Fractures serve as major conduits because their fluids can respond more rapidly to hydraulic overload than the more slowly moving pore fluids. Other lines of evidence for fresh-water discharge in the sea-water zone are the lower than expected salinities in the CALICA cenote which were limited to about 80% sea water at maximum depth (Figure 4).

The sea-water hydraulic head "$h_s$" for a CALICA borehole can be calculated if the equipotential lines are vertical and the depth to the brackish-water interface below the piezometric surface (ground-water table) is known (Domenico, 1972, equation 4.88).

$$h_s = [(p_s - p_f)z + p_f h_f]/p_s \qquad (3)$$

The equation assumes a sharp interface between the fresh-water and sea-water zones, which is approximated at CALICA by the 50% sea-water depth on Figures 2 and 4. Computed values of $h_s$ from equation (3), for the three boreholes for which $h_f + z$ are accurately known, are shown in parentheses on Figure 3. The assumption of vertical equipotential lines cannot be met in a dynamic system; however, the positive magnitude of the computed $h_s$ values (0.2 m) suggest that the "true" sea-water hydraulic heads are also positive, supporting the possibility of rising sea water. The decrease in sea-water hydraulic head in the southerly direction corresponds to the general direction of fresh-water hydraulic head decrease.

### *Point-Dilution Velocity Test*

Several point-dilution tests were conducted in the uncased P2 borehole in November in the fresh-water and sea-water regimes. The tests were made at depths of 6.1 and 16.5 m, respectively, below mean sea level (Figure 2), above and below the brackish-water interfaces. The results of two representative tests are shown on Figure 7. Field data followed the theoretical linear relationship [equation (1)] between time and the $\ln[(c - c^*)/(c^\circ - c^*)]$ until c approached the baseline conductivity of the ground water. The slopes of the best-fit linear lines on Figure 7 were used to compute velocities of 0.021 and 0.082 cm/sec, respectively, at the injection depths within the fresh-water and sea-water regimes. In the velocity calculations, the assumption is made that the borehole conductivity is constant across the diameter of the borehole (9.1 cm) and that flow and dispersion are not occurring in a vertical direction at the monitoring point. Vertical dispersion (due to density differences between the injected fluid and the ground water) and flow will decrease the time required to dilute the injected fluid, resulting in an overestimation of the ground-water velocity and specific discharge. Therefore, the velocity values reported within P2 represent the maximum velocities due to the positive error generated by assuming horizontal flow only.

The maximum November hydraulic head gradient around P2 (Figure 3b) is 13 cm/km between P3 and P2, indicating the general direction of fluid flow. A hydraulic conductivity of 65 cm/sec is computed from Darcy's law using the point-dilution velocity in the fresh-water zone with this hydraulic head gradient and an average porosity of 40%. The high value reflects flow through cavity voids associated with the dual-porosity nature of the limestone. Freeze and Cherry (1979, p. 156) note that dissolution can create passageways "causing local permeability to be almost infinite compared to other parts of the formation."

Wilson (1989) reported boreholes drilled near Caleta Xcaret penetrated an average of 12% cavity space. Because CALICA is only 1 km south of the Xcaret road, these boreholes are assumed representative of those drilled at CALICA. If we assume the fluid flow is primarily through fractures taking up 12% of the rock, the computed hydraulic conductivity using 12% porosity is 19 cm/sec.

The point-dilution velocities measured in P2 are of the magnitude to suggest fracture-flow influence at the two specific depths where velocities were measured. The P2 sea-water velocity was measured near a fracture as indicated by the decrease in salinity with depth in Figure 2. The higher velocity in the sea-water zone, relative to the fresh-water zone, probably reflects fracture flow at this point in the P2 borehole.

Darcy's law cannot be applied to determining the hydraulic conductivity within the sea-water/brackish-water regime affected by free convection, reflecting density differences (Domenico and Schwartz, 1990, p. 322). The measured sea-water velocity below the brackish/sea-water interface indicates a nonstatic state. Monitoring of the water table throughout a daily tidal cycle showed the P2 borehole is too far from the coast, 2.5 km, to be affected by the tides which have a maximum range of 30 cm (Cooper, 1959; Ford, 1985). The point-dilution method does not indicate the flow direction, but the previously computed sea-water hydraulic heads indicate flow below the brackish-water zone parallels the flow of fresh water towards the coast. This movement is shown schematically in Figure 6b, in which the

sea water is part of the return arm of a convection cell involving the inland movement of sea water at greater depths. The sea water eventually rises to replace sea water that contributes to the brackish-water zone and is subsequently discharged at the coast (Cooper, 1959).

### *Flow Meter Measurements in Cenotes the Coastal Region*

In Figure 8, the flow velocities are plotted as a function of depth for two coastal cenotes, Yalku and Tancah, and two inland cenotes, Maya Blue and Car Wash (Figure 1). For the depth profiles, the sea-water percentages were constant at Car Wash (4%) and showed linear increases with depth for Maya Blue (6 to 7%), Tancah (28 to 31%), and Yalku (34 to 45%). Maximum velocities increased from 1 cm/sec 10 km inland at Car Wash to 3 cm/sec two km inland at Maya Blue to 12 cm/sec at Tancah and Yalku near the coast. Maximum flow velocities equivalent to those measured at Tancah and Yalku were measured at Xcaret, another coastal cenote. The general direction of maximum flow velocity was towards the coast at each cenote. The lower velocities at the shallower depths within the cenotes are due to the proximity of the cenote walls above the cave entrance (Figure 8). Maximum discharge velocities at the coast are expected to be higher than those measured at the coastal cenotes which were about 100 meters from the coast. Whitaker and Smart (1990) report maximum discharge velocities of 40 cm/sec from an oceanic blue hole off the east coast of Andros Island.

Flow velocities at Naranjal and the Temple of Doom, inland cenotes between Car Wash and Maya Blue (Figure 1), were less than 1 cm/sec, indicating lateral heterogeneity in the form of secondary fractures which may or may not be connected to the main fracture-flow system in the region. James Coke, a professional cave diver at Akumal, has spent several years mapping the fracture-cave system extending from Car Wash to the coast. He reports the presence of numerous offshoot fractures which may pinch out (personal communication, 1990).

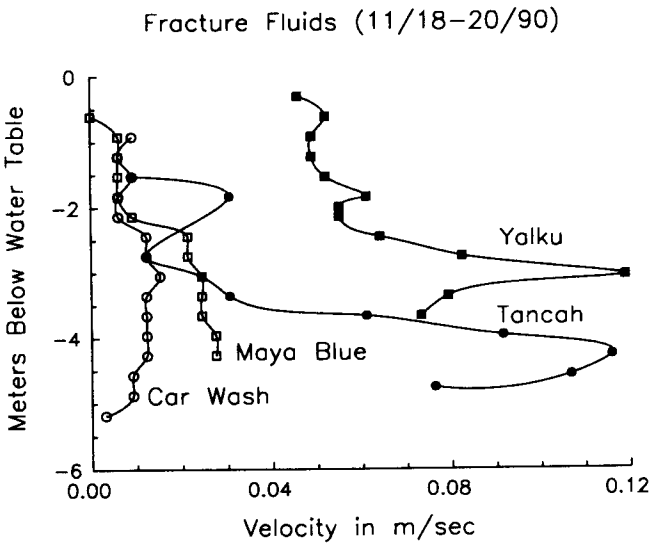


**Fig. 8. Depth profiles of flow velocity for cenotes in the coastal region in November 1990.**

The general increase in measured flow velocities in these large fractures as the coast is approached is due to two factors: the decrease in thickness of the fresh-water lens as it wedges out coastward and an overall increase in the volume of water passing through these fractures. The decrease in thickness of the fresh-water lens requires an increase in flow velocity to pass a constant volume of water. Another reason for the observed velocity increase approaching the coast is the funneling of additional water from smaller, secondary fractures into the larger fractures, increasing the volume of water passing through the larger fractures.

## Summary

Hydrological data were collected for a 70 km coastal section along the northeastern Yucatan coast. Measured velocities within large fractures in the fresh-water zone increased approaching the coast, from 1 to 12 cm/sec over a 10 km distance. The increase in flow velocity in the large fractures reflects the flow dynamics of a decreasing fresh-water lens width combined with the drainage of water from smaller, secondary fractures.

Velocities of 0.021 and 0.082 cm/sec were estimated from point-dilution tests in a borehole in the fresh-water and sea-water regimes, respectively, 2.5 km from the coast. These velocities reflect the influence of flow in fractures, especially for sea water in which the test was run near a fracture. Borehole hydraulic head gradients ranged from 10 to 15 cm/km in a region between 2 and 4 km from the coast. Hydraulic conductivities of 19 and 65 cm/sec, using 12 and 40% porosity, respectively, were calculated with Darcy's law for use in the fresh-water lens. Between 3.7 and 2.5 km from the coast, the average brackish-water zone (15 to 85% s.w.) increased in thickness from 1 to 2.2 m, and the average thickness of the overlying fresh-water zone decreased from 14 to 11.9 m.

The thickness of the fresh-water lens in the boreholes and in the CALICA cenote is approximately 40% less than that expected based on density differences between fresh water and sea water in a static system. The nonstatic fresh water is out of isostatic equilibrium with the underlying sea water, and thus has the potential to use fractures as conduits to inject fresh water below the halocline. Calculated positive sea-water hydraulic heads (assuming vertical equipotential lines) indicate the possibility of rising sea water. The general location of the halocline and the thickness of the fresh-water lens did not vary significantly between August and November. This apparent steady state may result from the rapid flow of fresh water and brackish water towards the coast (due to high transmissivity values resulting from fractures) combined with rising sea water at depth as part of convectional flow.

## Acknowledgments

This study represents a portion of the senior author's M.S. thesis. We appreciate the input of W. C. Ward and A. E. Weidie on the geology of Quintana Roo. John Clark provided access to the CALICA sites, and Jorge Rodriguez

Bremauntz helped collect the borehole data. James Coke of Akumal guided us to several of the cenotes and helped collect data. Yong Chen and Yang Chen helped collect the August field data. Partial field support was provided by Exxon Production Research Company.

## References

Back, W., B. B. Hanshaw, T. E. Pyle, L. N. Plummer, and A. E. Weidie. 1979. Geochemical significance of groundwater discharge and carbonate solution to the formation of Caleta Xel Ha, Quintana Roo, Mexico. Water Resources Research. v. 15, pp. 1521-1535.

Back, W. 1985. Hydrogeology of the Yucatan. In: Geology and Hydrogeology of the Yucatan and Quaternary Geology of Northeastern Yucatan Peninsula. New Orleans Geological Society, New Orleans, LA. 160 pp.

Back, W., B. B. Hanshaw, J. S. Herman, and J. N. Van Driel. 1986. Differential dissolution of a pleistocene reef in the ground-water mixing zone of coastal Yucatan, Mexico. Geology. v. 14, pp. 137-140.

Cooper, H. H., Jr. 1959. A hypothesis concerning the dynamic balance of freshwater and saltwater in a coastal aquifer. Journal of Geophysical Research. v. 64, pp. 461-467.

Domenico, P. A. 1972. Concepts and Models in Groundwater Hydrology. McGraw-Hill, New York, NY. 405 pp.

Domenico, P. A. and F. W. Schwartz. 1990. Physical and Chemical Hydrogeology. John Wiley & Sons, New York, NY. 824 pp.

Drost, W., D. Klotz, A. Koch, H. Moser, F. Neumaier, and W. Rauert. 1968. Point dilution methods of investigating ground water flow by means of radioisotopes. Water Resources Research. v. 4, pp. 125-146.

Ford, B. H. 1985. Geochemistry of water in a coastal mixing zone, northeastern Yucatan Peninsula (M.S. thesis). Univ. of New Orleans, New Orleans, LA. 90 pp.

Freeze, R. A. and J. A. Cherry. 1979. Groundwater. Prentice Hall, Inc., Englewood Cliffs, NJ. 604 pp.

Hubbert, M. K. 1940. The theory of ground-water motion. Journal of Geology. v. 48, pp. 785-944.

Moore, Y. H. 1991. Ground-water flow along the northeastern coast of the Yucatan Peninsula, Mexico (M.S. thesis). Univ. of New Orleans, New Orleans, LA. 54 pp.

Sanford, W. E. and L. F. Konikow. 1989a. Porosity development in coastal carbonate aquifers. Geology. v. 17, pp. 249-252.

Sanford, W. E. and L. F. Konikow. 1989b. Simulation of calcite dissolution and porosity changes in saltwater mixing zones in coastal aquifers. Water Resources Research. v. 25, pp. 655-667.

Sanford, W. E. and L. F. Konikow. 1989c. Reply on "Porosity development in coastal carbonate aquifers." Geology. v. 17, pp. 962-963.

Stoessell, R. K., W. C. Ward, B. H. Ford, and J. D. Schuffert. 1989. Water chemistry and $CaCO_3$ dissolution in the saline portion of an open-flow mixing zone, coastal Yucatan Peninsula, Mexico. Geological Society of America Bulletin. v. 101, pp. 159-169.

Ward, W. C. and R. B. Halley. 1985. Dolomitization in a mixing zone of near-seawater composition, late Pleistocene, northeastern Yucatan Peninsula. Journal of Sedimentary Petrology. v. 55, pp. 407-420.

Weidie, A. E. 1985. Geology of Yucatan Platform. In: Geology and Hydrogeology of the Yucatan and Quaternary Geology of Northeastern Yucatan Peninsula. New Orleans Geological Society, New Orleans, LA. 160 pp.

Whitaker, F. F. and P. L. Smart. 1990. Active circulation of saline ground waters in carbonate platforms: Evidence from the Great Bahama Bank. Geology. v. 18, pp. 200-203.

Wilson, W. L. 1989. Comment on "Porosity development in coastal carbonate aquifers." Geology. v. 17, pp. 961-962.

* * * * *

*Yolanda H. Moore graduated with an M.S. in Geology in May 1991 from the University of New Orleans. This paper represents her M.S. thesis study in hydrology. She previously worked for several independent oil companies in Shreveport while finishing her B.S. degree in Geology at Centenary College in 1989. Her professional interests are in Environmental Hydrology. She is currently employed as a hydrologist for URS Consultants, Inc., in Metairie, Louisiana.*

*Ronald K. Stoessell is a Professor of Geology at the University of New Orleans. He received his doctorate in Geology at the University of California at Berkeley in 1977. He then worked for one year as a research geologist for Exxon Production Research Company in Houston and four years as an Assistant Professor in the Coastal Studies Institute at Louisiana State University, before joining UNO in 1982. His research interests are in low-temperature geochemistry of water-rock interactions.*

*Dale H. Easley is an Assistant Professor of Geology at the University of New Orleans. He received his doctorate in Geology at the University of Wyoming at Laramie in 1989. He joined the UNO faculty in the Fall of 1989. His major research interests are in geostatistics, computer modeling, and in environmental geohydrology.*